DRY SLIDING FRICTION AND WEAR PROPERTIES OF Ti–TiC COMPOSITE FOAMS PREPARED BY SPARK PLASMA SINTERING AND DISSOLUTION PROCESS

Fan Lv,[1,2] Jie Zhang,[2] Chunxin Pan,[2] Nan Cao,[2] Jian Cao,[2] Jun Tian,[2,3] and Binna Song[2,3]

Ti–TiC composite foams were prepared by combining different volume fractions of TiC (0, 5, 10, and 15 vol.%) with NaCl as a space holder (20, 40, and 60 vol.%) by using spark plasma sintering (SPS) and a dissolution process. The sintering properties (relative density, porosity and microhardness), pore structure, friction and wear properties of the prepared foams were systematically studied. The Ti–TiC composite foams sintered at 700°C had an average pore diameter of approximately 230 μm. The microhardness of the Ti–10 vol.% TiC was significantly higher than that of porous Ti, with values ranging between 360.72 and 490.12 $HV_{0.2}$ recorded for the composite. The average coefficient of friction (COF) for the Ti–TiC composite foams was measured as 0.12–0.17 using a pin-on-disk tribometer. The lowest COF was obtained for a foam with a volume fraction of added NaCl (V_{NaCl}) of 40%. The wear rate of the examined foams was inversely related to their porosity, and the addition of TiC particles significantly improved the wear resistance of the porous Ti. The foams with 10 vol.% TiC exhibited the highest wear resistance, with a COF of 0.1349 and a wear rate of $0.65 \cdot 10^{-12} m^3 \cdot N^{-1} \cdot m^{-1}$. The wear mechanism of the Ti–TiC composite foams was a combination of adhesive and abrasive wear.

Keywords: *Ti–TiC composite foams, spark plasma sintering and dissolution, friction, porosity.*

INTRODUCTION

Porous titanium (Ti) has good structural properties, such as low weight and high specific strength, as well as excellent functional properties, including corrosion resistance and biocompatibility [1, 2]. Therefore, it is widely used in areas like aerospace and biomedicine [3–5]. However, porous Ti also has a low surface hardness, poor bearing capacity, and low elastic modulus and is prone to adhesive wear. Its surface is also prone to frictional damage and failure, especially under friction conditions [6–8]. Thus, Ti-based composite foams are generally reinforced with ceramic particles to improve their hardness, friction, and wear properties [9–12]. Among ceramic particles, the density and thermal expansion coefficient of titanium carbide (TiC) particles are similar to those of Ti. TiC particles have good chemical stability and compatibility with Ti and can therefore be effectively used to reinforce porous Ti, creating a Ti–TiC composite [13, 14].

[1]Soochow University, School of Mechanical and Electrical Engineering, Suzhou 215131, China. [2]Soochow University, School of Iron and Steel, Suzhou 215131, China.

[3]To whom correspondence should be addressed; e-mail: jtian@suda.edu.cn; songbinna@suda.edu.cn.

Spark plasma sintering (SPS) is commonly used to prepare Ti-based composites [15, 16]. Saliou et al. [17] used SPS to reinforce commercially pure titanium (CP-Ti) with TiC, titanium nitride (TiN), titanium carbon nitride (TiCN), and titanium diboride (TiB_2) phases. Ti–TiC composites with a high density and hardness were obtained using a low sintering temperature. Farías et al. [18] applied SPS to a titanium dihydride (TiH_2) mixture in a Ti matrix. The TiH_2 decomposed under heating to release H_2 and yield a low-porosity Ti–TiC composite foam. Zhang et al. [19] used SPS and dissolution to prepare Ti foams with porosity ranging from 30–70%.

To date, very few studies have been performed on the friction and wear performance of Ti-based foams. Liu et al. [20] used a pin-on-disk tribometer with a tungsten carbide (YG6) ball to study the wear of porous Ti, measuring an average coefficient of friction (COF) greater than 0.5. Farías et al. [18] used a pin-on-disk tribometer with an aluminum oxide (Al_2O_3) ball to study the wear of TiC-reinforced Ti-based materials, COF and wear volume changed as the fuction of TiC content. Bai et al. [10] used a pin-on-disk tribometer with a silicon nitride (Si_3N_4) ball to study the wear of TiC-reinforced Ti-based materials. The TiC particles provided support and created a barrier effect that delayed the wear of the Ti matrix. Thus, the Ti-based composites exhibited a reduced wear rate and significantly enhanced wear resistance compared to the Ti matrix. Pramanik [21] modified the percent of reinforcement phases and parameters of a wear system to delay its transition to a severe wear state, thereby improving the wear resistance of the system.

In this work, NaCl was used as a space holder in conjunction with added TiC particles to reinforce Ti-based materials [22]. For the Ti–TiC composite foams prepared by SPS and dissolution, the sintering properties were studied, the pore structure was characterized, and the volume fraction of added TiC (V_{TiC}) was optimized. Ti–TiC composite foams with uniformly dispersed TiC particles, tunable porosity, and a high relative density were prepared at low sintering temperatures. A pin-on-disk tribometer with preloaded aluminum oxide (Al_2O_3) pin was used to investigate the friction and wear properties and wear scar topography. The friction curve, average COF, and wear mechanism were analyzed.

This work systematically studied the effects of V_{TiC} and foam porosity on the friction and wear behavior of each composition and the wear mode under different friction conditions. The aims were to provide a reference for improving the friction and wear properties of Ti-based foams and experimental and theoretical bases for applying Ti-based foams under different friction conditions.

<center>EXPERIMENTAL PROCEDURES</center>

Materials. The CP-Ti (>99.6%, ~44 μm, Hebei Metal Materials), TiC (>99.2%, ~10 μm, Sinopharm Chemical Reagent Co., Ltd.), and NaCl (>99.5%, 150~300 μm, Tianjin Kemiou Chemical Reagent Co., Ltd.) powder as space holders were used in this work. Figure 1 shows the morphologies of Ti and TiC powders, displaying an irregular shape and a rugged surface, while the NaCl particles were cuboidal.

Fabrication Process. The following method was used to prepare Ti–TiC composite foams based on SPS and dissolution processes. Ti and TiC powders were first mixed in a prescribed ratio (corresponding to V_{TiC} percentages of 0, 5, 10, and 15%) and were then placed in a planetary ball mill (YXQM-1L, Mi Qi, China). Ball-milling was performed in an argon gas environment to prevent oxidation of the Ti powders. The ball-to-powder ratio was 10 : 1–5 : 1, the rotational speed was 250 rad/min, and the ball milling time was 10 h. Next, the mixed powder was loaded into a graphite mold and vacuum-sintered in an SPS furnace (LABOX-110, Sinter Land, Japan) at 700°C using a heating rate of 50°C/min, a holding time of 10 min, and a pressure of 30 MPa. A cylindrical composite with a diameter of 10 mm and a height of 5 mm was thus prepared. Finally, the Ti–TiC composite foam was held in water at 60°C for 24 h to dissolve the included NaCl, after which the specimen was dried at 100°C for 2 h.

Characterization. X-ray diffraction (XRD, Rigaku Ultima IV) was used for phase analysis based on the following main parameters: Cu-$K\alpha$ radiation, a scanning range of 20–80° (2θ°), and a step size of 0.02°. Scanning electron microscopy (SEM, Hitachi, SU-S500) was used to observe the microstructures of the powders, sintered samples, and worn surfaces, while energy-dispersive X-ray spectrometry (EDS, Oxford) was applied for elemental analysis.
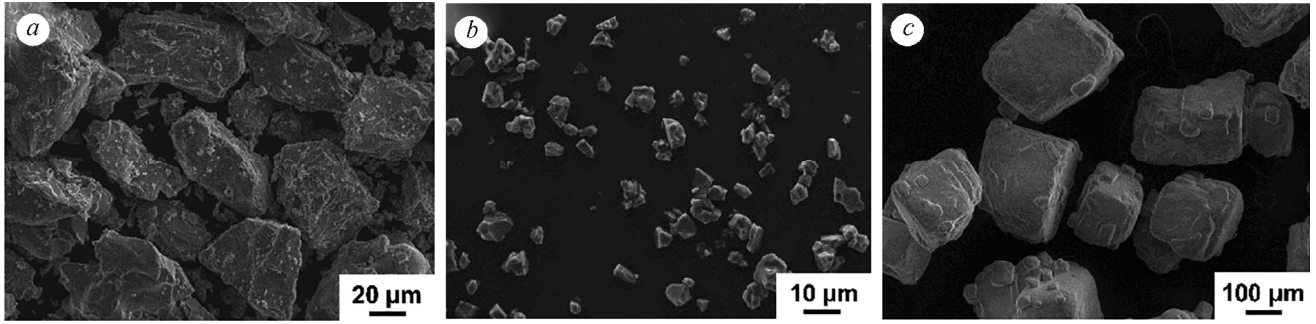
Fig. 1. SEM image of raw powders: *a*) Ti; *b*) TiC; *c*) NaCl

Pore sizes were measured using ImageJ software. Microhardness was measured using a micro-sclerometer (TH701, Time, China) with a 200 g and a loading time of 10 s. The true density of Ti–TiC composite foams was measured by the Archimedes method, and the relative density of the Ti–TiC matrix was calculated according to Eq. (1):

$$RD_{\text{Ti–TiC matrix}} = \frac{\rho_{\text{true}}}{(1\text{-}P_{\text{th}})\rho_{\text{sd}}}100\%, \tag{1}$$

where ρ_{true} is the true density of Ti–TiC composite foams; ρ_{sd} is the solid density of Ti–TiC composite using a rule of mixtures, and P_{th} is the theoretical porosity.
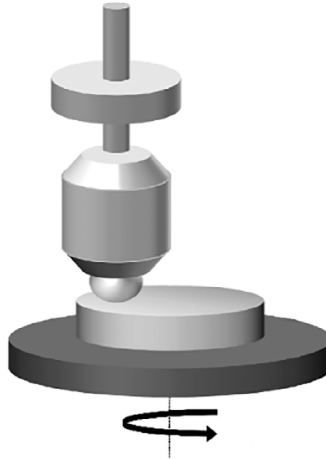
Fig. 2. Schematic diagram of the pin-on-disk test apparatus

Figure 2 presents a schematic of the employed pin-on-disk tribometer (MS-T3000, Lanzhou, China). Dry sliding wear tests were conducted in which an Al_2O_3 ball ($\Phi = 5$ mm, HV = 1740) was employed as the counterpart. The tests were carried out with two normal loads of 5 and 50 N, rotational speeds of 100 and 200 rpm, a friction track semi-diameter of 3 mm, and a total sliding time of 1800 s. A surface roughness tester (Surfcorder SE300, Kosaka, Japan) was used to measure the resulting wear-scar contour, from which the wear-scar depth was calculated. The sample mass was measured before and after the test, allowing the specific wear rate to be calculated:

$$W - \frac{V}{FS}, \tag{2}$$

where W is the specific wear rate ($mm^3/mm \cdot N$); V is the wear volume (mm^3); S is the sliding distances (mm), and F is the normal load.

Sintering Properties. Figure 3 shows the sintering properties of the Ti–TiC composite foams with different V_{TiC} percentages and volume fractions of added NaCl (V_{NaCl}). Figure 3*a* shows that the relative density of the Ti–TiC matrix (RD_{Ti-TiC}) sintered at 700°C was over 95%. The foams with V_{TiC} = 15% and V_{NaCl} = 20% had the lowest RD_{Ti-TiC}. The foams with 40% or more NaCl and 10% or less TiC had a RD_{Ti-TiC} greater than 98%. The porosity of the Ti–TiC composite (Fig. 3*b*) was approximately equal to that of the respective V_{NaCl} for foams with less than 10% TiC and slightly greater than that of V_{NaCl} for foams with 10% or more V_{TiC} because of the associated decrease in the relative density of the Ti–TiC matrix. Figure 3*c* shows the microhardness of the Ti–TiC composite foams. For samples with the same V_{TiC}, the microhardness decreased significantly as V_{NaCl} increased: the microhardness of samples with 60% NaCl was 17–26% lower than those with 20% NaCl. The microhardness was also measured for samples with the same V_{NaCl} and different V_{TiC} percentages. The microhardness of all samples with 5% TiC was approximately 20% greater than those without added TiC. The maximum microhardness (495.16 $HV_{0.2}$, 490.12 $HV_{0.2}$, and 360.72 $HV_{0.2}$) was obtained for the foams with 10% TiC. However, the lowest microhardness was obtained for the foam with 15% TiC, because a high V_{TiC} decreases the relative density of the Ti–TiC matrix after sintering and, therefore, its microhardness. Figure 3*d* is a map of the microhardness distribution over the vertical cross-section of a sample with 40% NaCl and 10% TiC. The relatively uniform microhardness distribution from the upper surface to the bottom of the samples indicates that a uniform composite structure can be prepared by the proposed process.

In summary, the two main influencing factors for the microhardness of the Ti–TiC matrix were the relative density and the TiC content. The Ti–TiC matrix of the Ti–10 vol.% TiC composite foams had a relatively high density (>96%). For samples with the same V_{NaCl} percentage, the Ti–10 vol.% TiC composite foams had the highest
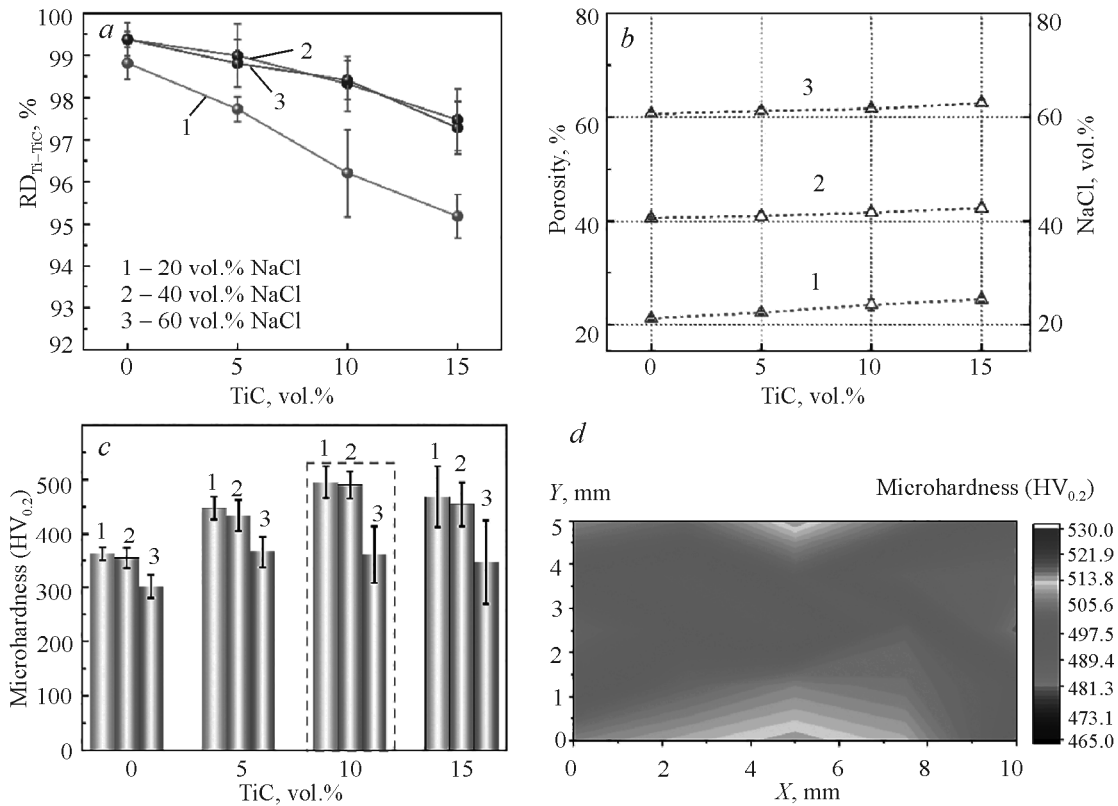
Fig. 3. Sintering properties of Ti–TiC composite foams: *a*) relative density of Ti–TiC matrix; *b*) porosity; *c*) microhardness; *d*) microhardness distribution feature through the vertical-section (40 vol.% NaCl, 10 vol.% TiC)
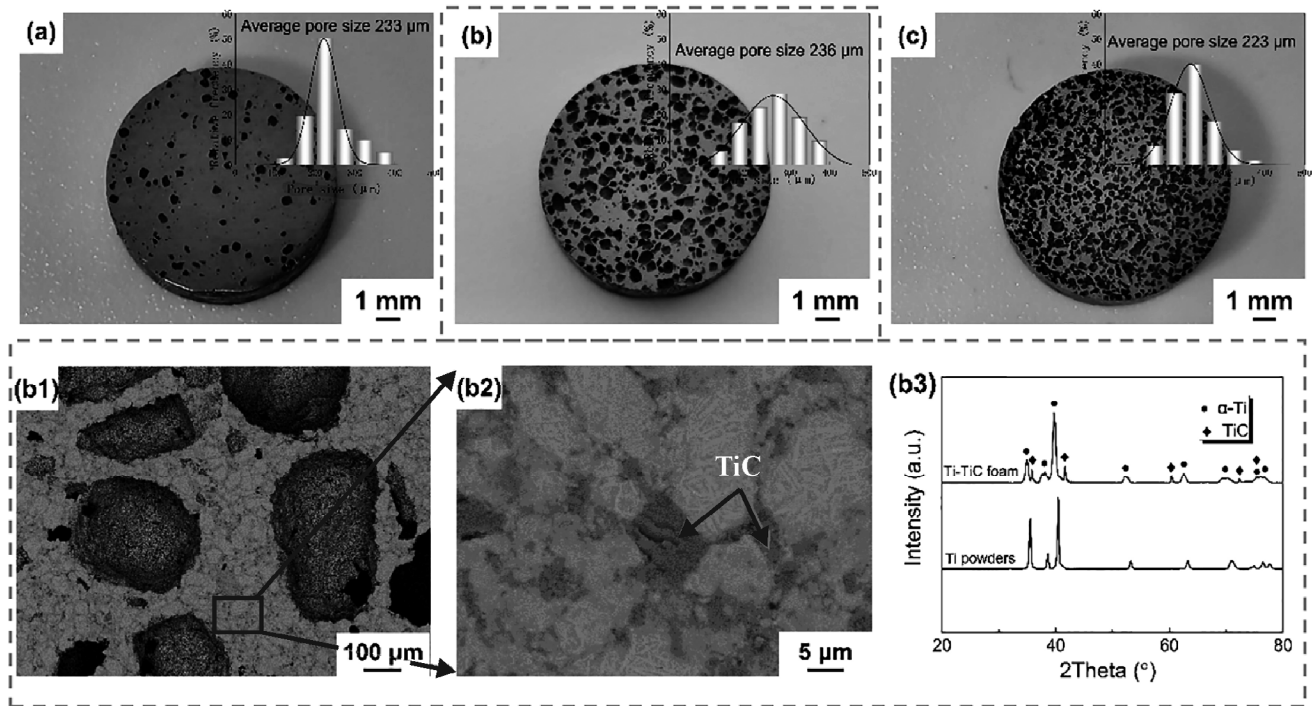
Fig. 4. Typical structure and pore size of distribution of Ti–10 vol.% TiC composite foams with 20 (*a*), 40 (b), and 60 vol.% NaCl (*c*): *b*1) microstructure of pore structure of the composite foams with 40% NaCl; *b*2) high magnification morphology of *b*1 position; *b*3) sintered samples of XRD

microhardness among the investigated foams. Based on these results, the Ti–10 vol.% TiC composite foams were subjected to further testing to analyze their friction and wear properties.

Pore Structure and Microstructure. Figure 4 shows the typical morphology and pore size distribution of Ti–10 vol.% TiC composite foams with different V_{NaCl} percentages. The pores on the surface of the composite foams were relatively uniformly distributed and mostly square-shaped. The average pore size was approximately 230 μm (Fig. 4*a–c*), which was consistent with the size and shape of the added NaCl. The microstructure and phase of the Ti–10 vol.% TiC composite foams with 40% NaCl were analyzed. Figure 4*b1* shows that the pores have distinct walls with good interconnections and smooth edges. The pores were mainly cubic, although the small number of circular pores observed was likely due to the shearing of a few NaCl particles into round shapes by the grinding balls during the mixing process [22]. Figure 4*b2* is a magnified portion of Fig. 4*b1* that illustrates the matrix morphology, with the dark regions corresponding to the TiC particles. The TiC particles were evenly distributed and well bonded to the Ti matrix. The XRD results presented in Fig. 4*b3* show that no intermediate compounds were generated.

Friction and Wear Properties. Figures 5*a–c* shows the friction and wear properties of the Ti–TiC composite foams with 40% NaCl and different V_{TiC} under a 5 N load and a rotational speed of 100 rpm. For the same counterpart, a small friction coefficient indicates a higher wear resistance for the abrasive material [23]. In the initial wear stage, the COFs of the porous Ti samples without TiC increased sharply to a maximum at a sliding time of approximately 90 s and then gradually decreased, where the average COF was 0.2343. By comparison, the COF of the Ti–TiC composite foams was significantly lower and averaged 0.1349–0.1507, as shown in Fig. 5*b*. The lowest wear rate calculated from Eq. (2) was $0.65 \cdot 10^{-12}$ m$^3 \cdot$ N$^{-1} \cdot$ m^{-1}. Compared to reported results for Ti samples with similar porosities, the COFs for porous Ti measured in this study were significantly lower, and the amount of wear was almost an order of magnitude lower [20]. Figure 5*c* shows a profile of a wear track. The relatively deep depression in the curve indicates a pore in the wear scar. After excluding any pore depths, the measured depth and width of the wear scars for porous Ti with different V_{TiC} percentages ranged from 65 to 36 μm
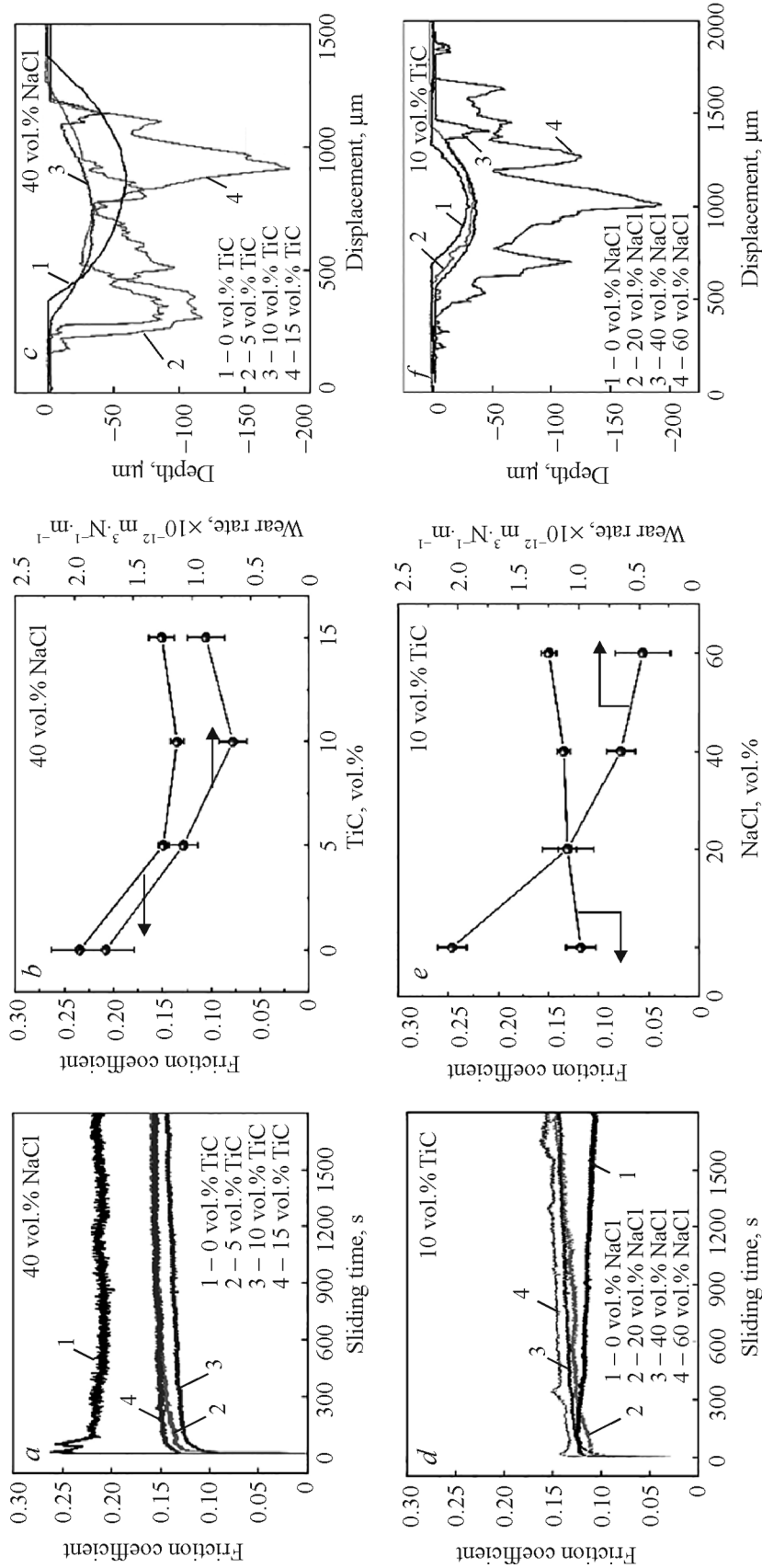
Fig. 5. Friction and wear properties of Ti–TiC composite foams of 40 vol.% NaCl at different TiC content: *a*) COF curves; *b*) average coefficient of friction and wear rate; *c*) profile of wear track. Friction and wear properties of Ti–10 vol.% TiC composite foams with different porosity: *d*) friction coefficient curves; *e*) average coefficient of friction and wear rate; *f*) profile of wear track

and 1310 to 879 μm, respectively. The foam with 10% TiC exhibited the lowest average COF (0.1349) and the smallest wear scar depth and width, which were approximately 55 and 67% lower, respectively, than those of porous Ti without TiC. Although the addition of TiC particles significantly improved the wear resistance of the material, the density and plasticity of the matrix decreased with increasing V_{TiC}. Therefore, the Ti–15 vol.% TiC foam had a lower wear resistance than the Ti–10 vol.% TiC foam.

Figure 5*d–f* shows the friction and wear properties of the Ti–10 vol.% TiC composite foams with different V_{NaCl} percentages. In the initial wear stage, the COF increases rapidly to reach a maximum at a sliding time of approximately 120 s. The following results were obtained for the Ti–10 vol.% TiC composite foams. The COF trended slightly upward over the sliding time. The average COF increased with the porosity, ranging from 0.1179 to
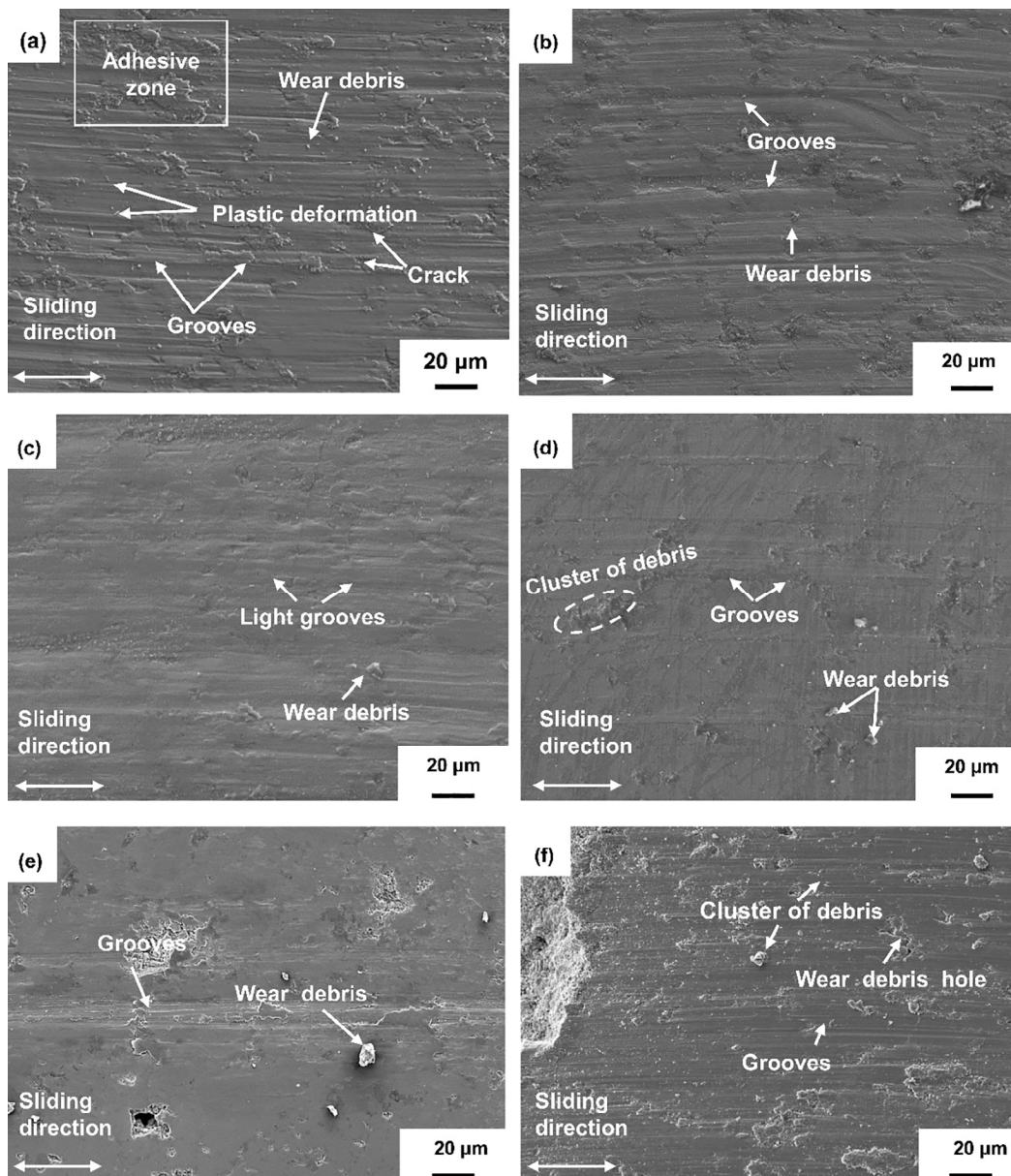
Fig. 6. Wear track images of Ti–TiC composite foams: *a*) 40 vol.% NaCl, Ti foam; *b*) 40 vol.% NaCl, Ti–5 vol.% TiC composite foams; *c*) 40 vol.% NaCl, Ti–10 vol.% TiC composite foams; *d*) 40 vol.% NaCl, Ti–15 vol.% TiC composite foams; *e*) 20 vol.% NaCl, Ti–10 vol.% TiC composite foams; *f*) 60 vol.% NaCl, Ti–10 vol.% TiC composite foams
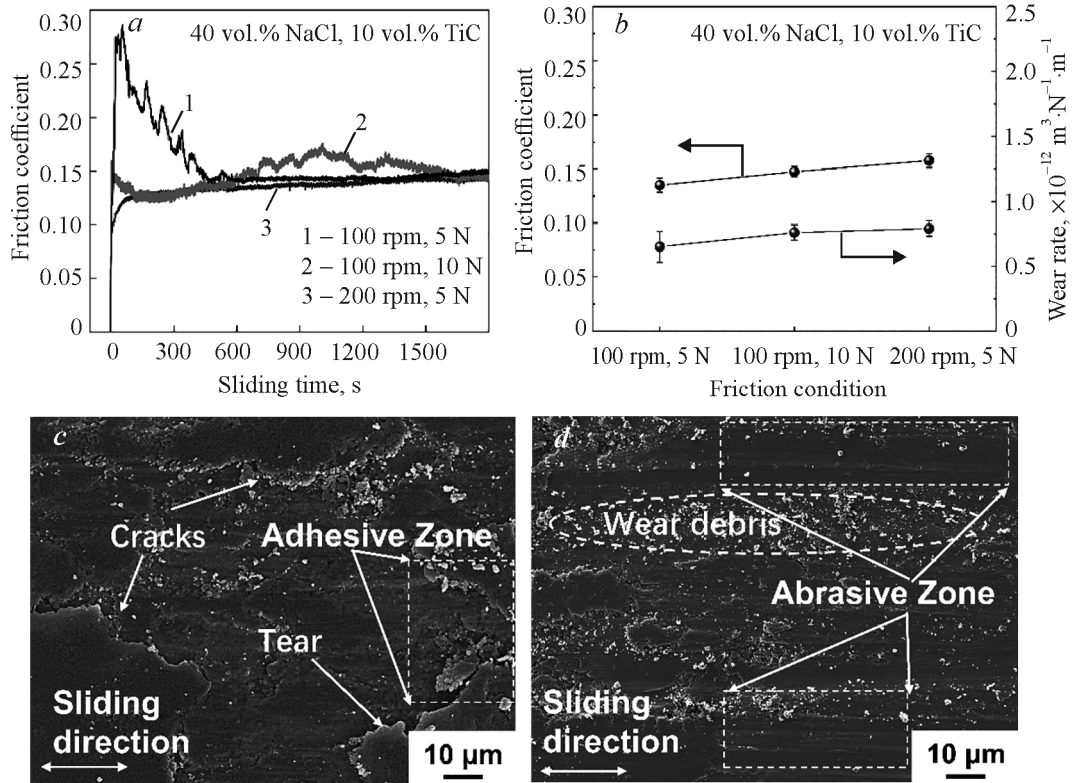
Fig. 7. Friction and wear properties of Ti–10 vol.% TiC composite foams of 40 vol.% NaCl under different load and speed: *a*) COF curves; *b*) average COF; *c*) wear morphology for 10 N, 100 rpm; *d*) 5 N, 200 rpm

0.1498. The wear rate decreased with increasing porosity and the wear rate of the samples with 40% NaCl was approximately 23% of the wear rate of the solid Ti–TiC composites. The contact area in the friction test decreased as the porosity increased, resulting in a decrease in the wear rate of the samples under the same friction conditions. Figure 5*f* shows that as the porosity increases, the wear-scar depth increases from approximately 29 to 50 μm, and the wear-scar width increases from around 651 to 1298 μm. These results were obtained because porous materials have a lower resistance to plastic deformation than solid materials, resulting in simultaneous damage in the horizontal and longitudinal directions along the contact surface.

Figure 6 shows the corresponding wear track topography under the same conditions as for Fig. 5. In Fig. 6*a*, the surface of porous Ti without added TiC has many parallel grooves in the sliding direction that are deeper than the grooves on the surface of the samples with added TiC, measuring approximately 10–20 μm in width. There is a localized adhesive zone (white box). Because porous Ti has relatively good plasticity and low hardness, localized plastic crushing could occur on the contact surface, resulting in adhesion between the surface and material fragments. Repeated frictional rubbing can cause wear debris to be pulled off the worn surface. Some large wear debris is extruded by the friction pair and attached to the wear scars, whereas some small wear debris creates numerous grooves due to sliding friction between the friction pair and wear scars. At this stage, the main wear mechanism is adhesive wear [23]. However, Figs. 6*b–e* shows that as V_{TiC} increases, the groove width gradually decreases, and the amount of wear debris significantly decreases. The maximum microhardness (495.16 $HV_{0.2}$, 490.12 $HV_{0.2}$, and 360.72 $HV_{0.2}$) was obtained for the foams with 10% TiC particles act as a hard phase that blocks the action of friction, hindering deformation and protecting the matrix from damage, as indicated by the Archard equation [24]:

$$Q \propto \frac{1}{H},$$ (3)

323
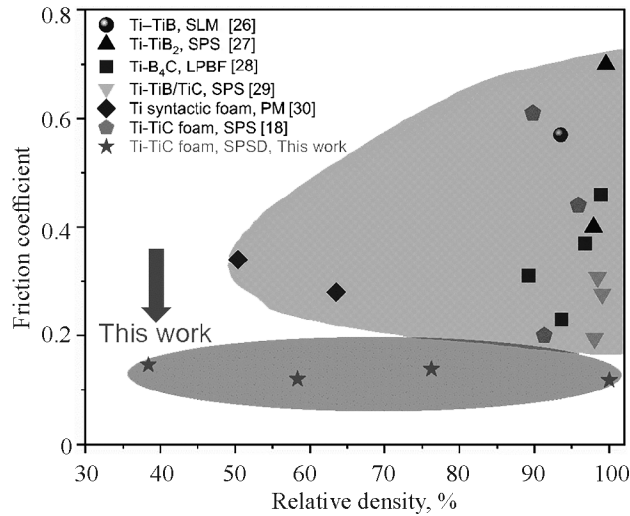
Fig. 8. Comparison of COFs [26–30]

where Q is the wear volume, and H is the surface hardness. The Ti–10 vol.% TiC composite foams with 40% NaCl had good wear resistance.

Figure 6*d* shows that for the Ti–15 vol.% TiC foam, an increase in the cluster of debris causes an increase in the wear rate compared to the foam without adding TiC. The Ti–10 vol.% TiC foam with 60% NaCl has a thinner pore wall than porous Ti, and weakly bound residual TiC particles tend to flake off under the action of friction, producing large pieces of abrasive debris. Figure 6*f* shows that during the friction process, three-body abrasive wear occurs, repeated friction creates more abrasive debris, the wear rate increases to $0.88 \cdot 10^{-12}$ m$^3 \cdot$ N$^{-1} \cdot$ m^{-1}, and the wear resistance of the material decreases. In conclusion, the primary wear mechanism of Ti–TiC composite foams is a mixture of adhesive and abrasive wear.

Figure 7 shows the friction and wear properties and wear track topography of the Ti–10 vol.% TiC composite foams with 40% NaCl under different loads and rotational speeds. Increasing the load from 5 to 10 N extends the running-in wear stage of the friction curve to approximately 120 s. Figures 7*a*, *b* show that the COF exhibits large fluctuations during the stable wear stage, increasing the average friction coefficient. Figure 7*c* shows the wear track topography, where numerous spalled layers of metal are generated mainly due to strong cutting and extrusion by the friction pair on the sample surface, which gradually increases the effect of adhesive wear [23, 25]. This phenomenon is also the main reason large COF fluctuations persist during the stable wear stage. Increasing the rotational speed from 100 to 200 rpm results in the running-in wear stage of the COF curve extending to approximately 480 s before the stable wear stage is entered. The COF over the stable stage is close to 100 rpm. The wear track topography presented in Fig. 7*d* shows that more debris is produced under the friction condition of the high rotational speed. Because of the debris, more time is required to realize a stable contact between the pin and the sample surface during the running-in wear stage, which leads to large fluctuations in the COF during this phase, making abrasive wear the primary wear mechanism under a high rotational speed.

Figure 8 shows that the prepared material has a significantly lower COF than other Ti-based materials.

CONCLUSIONS

SPS and dissolution were used to prepare Ti–TiC composite foams with an average pore diameter of approximately 230 μm and a Ti–TiC matrix uniform relative density greater than 95%.

The addition of TiC particles significantly improved the microhardness of porous Ti. The microhardness of the Ti–TiC composite foams ranged from 360.72 to 490.12 HV$_{0.2}$ and was greatest for the Ti–10 vol.% TiC composite foam.

The average COF of the Ti–TiC composite foams was 0.12–0.17. The addition of TiC particles improved the wear resistance of porous Ti. The material porosity considerably impacted the COF. The lowest COF of the Ti–TiC composite foams was obtained for 40% NaCl, and the wear rate was inversely related to the porosity. The Ti–10 vol.% TiC composite foam with 40% NaCl exhibited the best wear resistance, with a COF of 0.1349 and a wear rate of $0.65 \cdot 10^{-12}$ m$^3 \cdot$ N$^{-1} \cdot$ m^{-1}. The wear mechanism of the Ti–TiC composite foams was a mixture of adhesive and abrasive wear.

The wear rate of the Ti–10 vol.% TiC composite foams with 40% NaCl increased with the load and rotational speed. The main wear mechanism was adhesive wear under a high load of 10 N and a rotational speed of 100 rpm and abrasive wear under a load of 5 N and a high rotational speed of 200 rpm.

ACKNOWLEDGMENTS

AUTHOR CONTRIBUTIONS

Fan Lv: conceptualization, methodology, validation, investigation, visualization, writing-original draft. **Jie Zhang, Chunxin Pan, Nan Cao, and Jian Cao**: software, investigation, visualization. **Jun Tian and Binna Song**: conceptualization, writing-review and editing, supervision, funding acquisition.

REFERENCES

1. C. Leyens and M. Peters, "*Titanium and Titanium Alloys: Fundamentals and Applications*," Wiley-VCH Weinheim; John Wiley distributor, Chichester (2003).

2. H. Attar, S. Ehtemam-Haghighi, N. Soro, D. Kent, and M. Dargusch, "Additive manufacturing of low-cost porous titanium-based composites for biomedical applications: Advantages, challenges and opinion for future development," *J. Alloys Compd.*, **827**, 154263 (2020); DOI: 10.1016/j.jallcom.2020.154263.

3. Jia Jian-gang, Jin Ying-zhi, Gao Chang-qi, Liu Chang, Ji Gen-shun, Guo Tie-ming, "Preparation and development of porous titanium materials for bone transplantation," *Chinese J. Nonferr. Met.*, **29**, No. 6, 1187–1197 (2019); DOI: 10.19476/j.ysxb.1004.0609.2019.06.07.

4. Zheng Jing-pu, Chen Liang-jian, Chen Dai-yuan, Chao Chun-sheng, Yi Man-fei, Zhang Bo, "Effects of pore size and porosity of surface-modified porous titanium implants on bone tissue ingrowth," *Trans. Nonferr. Met. Soc.*, **29**, No. 12, 2534–2545 (2019); DOI: 10.1016/S1003-6326(17)60225-5.

5. B. Song and J. Cao, "Sintering properties of in situ Ti–TiB microlattices created by 3D extrusion printing of TiH$_2$ + TiB$_2$ inks," *J. Cent. South Univ.*, **28**, No. 4, 1078–1088 (2021); DOI: 10.1007/s11771-021-4681-2.

6. Yang Rui, Ma Wei, Wang Chao, Wang Ting-mei, and Wang Qi-hua, "Effect of hot rolling on microstructure and tribology behaviors of Ti–50.8 Ni alloy," *Trans. Nonferr. Met. Soc. China*, No. 4 (2021); DOI: 10.1016/S1003-6326(21)65553-X.

7. Zhu Yan-song, Liu Yun-fei, Wei Xing-nong, Sun Dong, Lu Wen zhuang, and Ko Tae Jo, "Tribological characteristics of the dual titanium boride layers (TiB$_2$ + TiB) on titanium alloy," *Ceram. Int.*, **47**, No. 10, 13957–13969 (2021); DOI: 10.1016/j.ceramint.2021.01.265.

8. H. Dong, Tribological properties of titanium-based alloys. *Surface Engineering of Light Alloys*, Elsevier (2010), pp. 58–80; DOI: 10.1533/9781845699451.1.58.

9. Bowen Zheng, Fuyu Dong, Xiaoguang Yuan, Yue Zhang, Hongjun Huang, Xiaojiao Zuo, Liangshun Luo, Liang Wang, Yanqing Su, Xuan Wang, and Peter K Liaw, "Investigation on microstructures and mechanical behavior of *in-situ* synthesized TiC and TiB reinforced Ti6Al4V based composite," *Mater. Res. Express*, No. 6, 116597 (2019); DOI: 10.1088/2053-1591/ab499d.

10. M. Bai, R. Namus, Y. Xu, D. Guan, W.M. Rainforth, and B.J. Inkson, "*In-situ* Ti–6Al–4V/TiC composites synthesized by reactive spark plasma sintering: processing, microstructure, and dry sliding wear behavior," *Wear*, **432–433**, 202944 (2019); DOI: 10.1016/j.wear.2019.202944.

11. Huang Lu-jun, An Qi, Geng Lin, Wang Shuai, Jiang Shan, Xiping Cui, Zhang Rui, Sun Fengbo, Jiao Yang, Chen Xin, and Wang Cunyu, "Multiscale architecture and superior high-temperature performance of discontinuously reinforced titanium matrix composites," *Adv. Mater.*, **33**, No. 6, 2000688 (2021); DOI: 10.1002/adma.202000688.

12. M.D. Hayat, H. Singh, Z. He, and Cao Peng, "Titanium metal matrix composites: An overview," *Comp. Part A: Appl. Sci. Manufact.*" **121**, 418–438 (2019).

13. Song Bin-na, C. Kenel, and D.C. Dunand, "3D ink-extrusion printing and sintering of Ti, Ti–TiB, Ti–TiC microlattices," *Addit. Manufact.*, **35**, 101412 (2020); DOI: 10.1016/j.addma.2020.101412.

14. Hooyar Attar, Shima Ehtemam-Haghighi, Damon Kent, Matthew S. Dargusch, "Recent developments and opportunities in additive manufacturing of titanium-based matrix composites: A review," *Int. J. Mach. Tools Manufact.*, **133**, 85–102 (2018); DOI: 10.1016/j.ijmachtools.2018.06.003.

15. O.E. Falodun, B.A. Obadele, S.R. Oke, A.M. Okoro, and P.A. Olubambi, "Titanium-based matrix composites reinforced with particulate, microstructure, and mechanical properties using spark plasma sintering technique: a review," *Int. J. Adv. Manufact. Technol.*, **102**, 1689–1701 (2019); DOI: 10.1007/s00170-018-03281-x.

16. Liu Kai-ge and Hu Shu-bing, "Microstructure evolution and enhanced bioactivity of (Ti–35Nb–7Zr–5Ta)–15HA biocomposites by spark plasma sintering," *Chinese J. Nonferr. Met.*, **30**, No. 1, 112–121 (2020); DOI：10.11817/j.ysxb.1004.0609.2020-39490.

17. S. Diouf, M.O. Durowoju, M.B. Shongwe, and P.A. Olubamb, "Processing of pure titanium containing titanium-based reinforcing ceramics additives using spark plasma sintering," *Leonardo Electr. J. Pract. Technol.*, **16**, No. 30, 269–286 (2017).

18. I. Farías, L. Olmos, O. Jiménez, M. Flores, A. Braem, and J. Vleugels, "Wear modes in open porosity titanium matrix composites with TiC addition processed by spark plasma sintering," *Trans. Nonferr. Met. Soc. China*, **29**, Issue 8, 1653−1664 (2019); DOI: 10.1016/S1003-6326(19)65072-7.

19. F. Zhang, E. Otterstein, and E. Burkel, "Spark plasma sintering, microstructures, and mechanical properties of macroporous titanium foams," *Adv. Eng. Mater.*, **12**, No. 9, 863–872 (2010); DOI: 10.1002/adem.201000106.

20. Z. Liu, F. Ji, M. Wang, and T. Zhu, "Study on the tribological properties of porous titanium sliding against tungsten carbide YG6," *Metals*, **7**, No. 1, 28 (2017); DOI: 10.3390/met7010028.

21. A. Pramanik, "Effects of reinforcement on wear resistance of aluminum matrix composites," *Trans. Nonferr. Met. Soc. China*, **26**, No. 2, 348−358 (2016); DOI: 10.1016/S1003-6326(16)64125-0.

22. N. Jha, D.P. Mondal, M.J. Dutta, Badkul Anshul, A.K. Jha, and A.R. Khare, "Highly porous open cell Ti-foam using NaCl as temporary space holder through powder metallurgy route," *Mater. Design*, **47**, 810–819 (2013); DOI: 10.1016/j.matdes.2013.01.005.

23. J.F. Archard, "Contact and rubbing of flat surfaces," *J. Appl. Phys.*, **24**, No. 8, 981−988 (1953); DOI: 10.1063/1.1721448.

24. A.T. Tabrizi, H. Aghajani, H. Saghafian, and F.F. Laleh, "Correction of Archard equation for wear behavior of modified pure titanium," *Tribology Int.,* **155**, 106772 (2021); DOI: 10.1016/j.triboint.2020.106772.

25. D. Cree and M. Pugh, "Dry wear and friction properties of an A356/SiC foam interpenetrating phase composite," *Wear*, **272**, No. 1, 88–96 (2011); DOI: 10.1016/j.wear.2011.07.008.

26. N. Kang, P. Coddet, Q. Liu, H. Liao, and C. Coddet, "In-situ TiB/near α Ti matrix composites manufactured by selective laser melting," *Addit. Manufact.*, **11**, 1–6 (2016); DOI: 10.1016/j.addma.2016.04.001.

27. A.S. Namini, M. Azadbeh, and M.S. Asl, "Effect of TiB_2 content on the characteristics of spark plasma sintered Ti–TiB_w composites," *Adv. Powder Technol.*, **28**, No. 6, 1564–1572 (2017); DOI: 10.1016/j.apt.2017.03.028.

28. Xia MU-jian, Liu Ai-hui, Lin Yue-bin, Li Nianlian , Ding Hongyan**,** Zhong Chen, "Densification behavior, microstructure evolution and fretting wear performance of in-situ hybrid strengthened Ti-based composite by laser powder-bed fusion," *Vacuum*, **160**, 146–153 (2019); DOI: 10.1016/j.vacuum.2018.11.023.

29. V.S. Balaji and S. Kumaran, "Dry sliding wear behavior of titanium-(TiB+TiC) in situ composite developed by Spark Plasma Sintering," *Tribol. Trans.*, **58**, No. 4, 698–703 (2015); DOI: 10.1080/10402004.2014.993780.

30. D.P. Mandala, M.D. Dutta, R.K. Bhartib, and M.J. Dutta, "Microstructural characterization and property evaluation of titanium cenosphere syntactic foam developed by powder metallurgy route," *Powder Metall.*, **58**, No. 4, 289–299 (2015); DOI: 10.1179/1743290115Y.0000000012.